Appl. Phys. A (2016) 122:453
DOI 10.1007/s00339-016-0004-0

Applied Physics A
Materials Science & Processing

Low-reflectance laser-induced surface nanostructures created with a picosecond laser

Shashank Sarbada[1] · Zhifeng Huang[2] · Yung C. Shin[1] · Xiulin Ruan[2]

Received: 8 January 2016 / Accepted: 14 March 2016 / Published online: 29 March 2016

Abstract Using high-speed picosecond laser pulse irradiation, low-reflectance laser-induced periodic surface structures (LIPSS) have been created on polycrystalline silicon. The effects of laser fluence, scan speed, overlapping ratio and polarization angle on the formation of LIPSS are reported. The anti-reflective properties of periodic structures are discussed, and the ideal LIPSS for low surface reflectance is presented. A decrease of 35.7 % in average reflectance of the silicon wafer was achieved over the wavelength range of 400–860 nm when it was textured with LIPSS at high scan speeds of 4000 mm/s. Experimental results of broadband reflectance of silicon wafers textured with LIPSS have been compared with finite difference time domain simulations and are in good agreement, showing high predictability in reflectance values for different structures. The effects of changing the LIPSS profile, fill factor and valley depth on the surface reflectance were also analyzed through simulations.

1 Introduction

With the growing need for renewable energy sources, there is an increasing demand for cheap and high-efficiency solar cells. Although high-efficiency silicon solar cells with overall efficiencies over 25 % [1] have been fabricated in laboratories, the high cost involved in manufacturing these high-efficiency devices makes their commercial use impractical. Optical losses through front surface reflections lower the overall efficiency of solar cells since bare silicon reflects nearly 40 % of incident solar radiation over the wavelength range of 200–1100 nm. Texturing the surface of silicon wafers to suppress reflections has been commonly used to improve the efficiency of solar cells [2–5]. Surface structures such as silicon nano-wire arrays [6], moth eye structures [7], nano-pyramids [8], nano-cones [9] and nano-domes [10] have been shown to greatly suppress surface reflections but are expensive to manufacture.

Grating structures are also known to exhibit anti-reflective properties [11–15]. The wavelength range over which they suppress surface reflections is influenced by the geometry of the grating [16]. These structures are commonly used to create anti-reflective coatings by methods such as mechanical scribing, lithography, etching, spin coating replication and vapor deposition [16–19]. Another method to create grating-like structures is through the formation of laser-induced periodic surface structures (LIPSS) which was first observed in 1965 [20]. LIPSS have been created using different types of lasers, both continuous wave [21] and pulsed beams of varying pulse durations and of different wavelengths [22–30]. They have been reported on many materials including metals [31, 32], dielectrics [33, 34], semiconductors [35], ceramics [36, 37] and polymers [38, 39]. Ripple structures having a period nearly equal to the wavelength of incident radiation have been reported in several studies. These are commonly referred to as low special frequency LIPSS (LSFL) and are formed orthogonal to the direction of the polarization of the laser [40–46]. LIPSS with periods significantly shorter than the wavelength of the laser have also been commonly

✉ Yung C. Shin
shin@purdue.edu

[1] Center for Laser-based Manufacturing, School of Mechanical Engineering, Purdue University, West Lafayette, IN 47907, USA

[2] School of Mechanical Engineering and Birck Nanotechnology Center, Purdue University, West Lafayette, IN 47907, USA

reported in the literature and are formed when ultra-short-pulsed lasers are used. These are known as high special frequency LIPSS (HSFL) and are oriented parallel or perpendicular to the direction of polarization [22, 40–42, 47–49]. The formation of LSFL was earlier attributed to the interference between the incident laser radiation and the surface scattered waves but was later improved by the efficacy factor theory of Sipe et al. [50]. The formation of HSFL is still not fully explained but has been attributed to the redistribution of the electric field over the surface due to the formation of LSFL [51].

In this work, low-reflectance LSFL have been created on the surface of silicon wafers at high scan speeds of 4000 mm/s. Although there have been many studies on the anti-reflective properties of LIPSS [52] created by femtosecond lasers, little work has been done in this area using picosecond lasers. Moreover, LIPSS formed by a picosecond laser has not been reported at high scan speeds exceeding 3000 mm/s, which is an important attribute to lowering the fabrication costs of solar cells. In addition, the anti-reflective properties of large area LIPSS created with low overlapping ratios of less than 65 % have been rarely reported, which are addressed in this work. This study also reports the effects of different grating profiles commonly observed in LIPSS on surface reflectance, using finite difference time domain (FDTD) simulations. In addition, the effect of varying the fill factor and valley depth of gratings on the reflectance is analyzed and reported.

2 Experimental details

A Lumera Rapid Picosecond laser was used to create LIPSS on silicon wafers. The laser generates linearly polarized pulses with a pulse duration of 10 ps at 1064 and 532 nm with a variable repetition rate ranging from 10 to 640 kHz. A half wave plate was used to rotate the angle of polarization. A beam expander was used to create a collimated and expanded beam which was directed into a laser scanner head. The scanner head contains high-speed mirrors and an 80 mm focal length objective lens. The laser beam focal spot size used was 10 µm. A computer controlled precision 3-axis stage was used to position the silicon sample under the scanner head. The silicon samples used are 127 mm diameter, 525 µm-thick polished wafers. The silicon is N doped with phosphorous, and its crystal orientation is (111) with the electrical resistivity less than 0.006 ohm-cm. In order to create LIPSS, the laser was scanned over the surface of the wafer, which was positioned at the focal length of the objective lens. Long scans were made in the x direction with small shifts in the y direction to create a large scanned area. All experiments were conducted with ambient air as the irradiation atmosphere.

To study the surface structures created on the sample, preliminary observations were made using an optical microscope, followed by SEM imaging. The samples were first cleaned in an ultrasonic cleaner with acetone, followed by methanol to dislodge loose particles and to free the sample from organic impurities that may have been present. Due to the low electrical conductivity of the sample, charging was expected during SEM imaging. To prevent charging, the silicon samples were sputter coated with platinum before imaging. AFM imaging was also done to study the profile of the structures formed. In order to study the composition and crystallinity of the silicon wafer before and after the creation of LIPSS on the surface, EDS and XRD analyses were performed.

In order to measure the broadband reflectance of the sample, a Perklin Elmer Lambda 950 spectrophotometer with an integrating sphere accessory was used. First, the sample was checked for opacity, and then, the spectral reflectance (R) and transmittance (T) were measured over the wavelength range of 200–1200 nm. A monochromator was used to resolve the wavelength. A blank wafer with no texturing was used to calibrate the machine, and its reflectance values were used for comparison with textured samples.

3 Results and discussion

Initial experiments to determine the parameters needed to achieve uniform LIPSS on the large area of silicon surface were conducted at a laser wavelength of 1064 nm. At a fluence value of 0.8 J/cm^2, uniform LIPSS were created on a small area. SEM and AFM imaging was done to study the

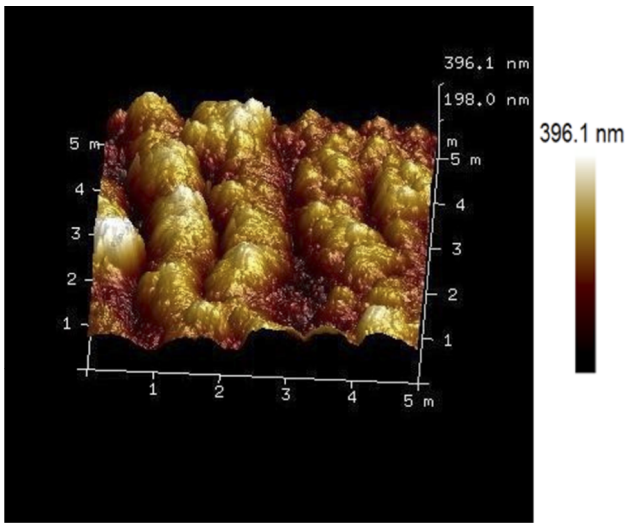

Fig. 1 AFM image of LIPSS created using a 1064 nm wavelength laser showing maximum valley depth

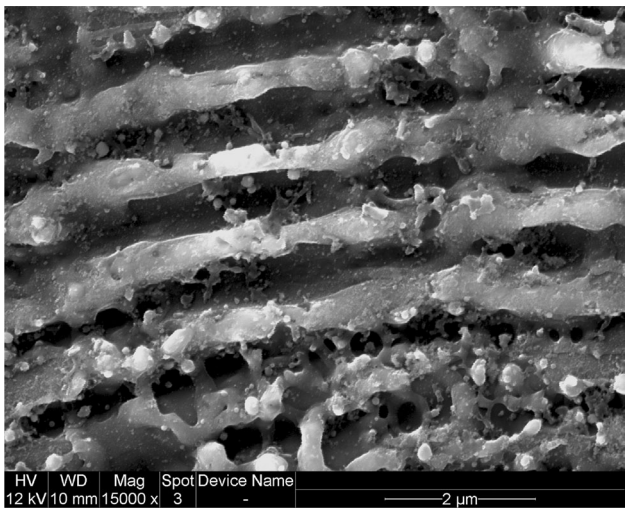

Fig. 2 SEM image of LIPSS created using a 1064 nm wavelength laser

profile and geometry of the structures. Figure 1 shows an AFM image of the LIPSS created at 1064 nm wavelength. The average valley depth was measured to be 300 nm, while the maximum valley depth was nearly 400 nm. As expected, the structures had a period of 1064 nm, which was the same as the wavelength of the laser used. Figure 2 shows an SEM image of LIPSS created using a 1064 nm wavelength laser.

In order to determine the period required to achieve the lowest surface reflectance, FDTD simulations were conducted. The simulation setup is described in detail in Sect. 3.3. The period of the grating structures was varied, and the effect on reflectance was studied. When the period was varied from 1100 to 400 nm in steps, it was determined that a period close to 450 nm was the most effective in suppressing reflections in the wavelength range of 200–1100 nm. This is the range of wavelengths in which silicon solar cells convert light energy to electrical energy. Since LSFL have a period nearly equal to the wavelength of incident laser radiation, the 532 nm wavelength of the picosecond laser was chosen. The focus in this study was to suppress reflections in the range of 400–860 nm, which is a range of high solar intensity for silicon solar cells. The 532 nm laser pulses were scanned over the silicon wafer at a repetition rate of 10 kHz. The scan speed was increased to gradually reduce the overlapping ratio from 99.9 to 50 %. The power was simultaneously increased to maintain the fluence required to form LIPSS. It was observed that uniform LIPSS could be generated for overlapping ratios ranging from 99.9 % down to 60 %. Below 60 %, gaps appeared between adjacent pulses and the LIPSS became discontinuous. In order to maximize processing speed, an overlapping ratio of 60 % was chosen and a scan speed of 60 mm/s was maintained. Uniform LIPSS over a large area were created through parallel line scans with small shifts normal to the scanning direction, while maintaining the overlapping ratio.

To study the effects of changing the laser beam polarization angle, a half wave plate was used in the beam path. The wave plate was rotated to change the angle of polarization, and the resultant LIPSS were studied. Varying the angle of polarization resulted in a change in the orientation of LIPSS without a change in the LIPSS period or profile. As the polarization angle was rotated from being normal to the scanning direction to being parallel to the scanning direction, the LIPSS was rotated by 90°. When the LIPSS were no longer parallel to the scan direction, it became necessary for the pulses in the adjacent parallel scan lines to be aligned such that continuous LIPSS could be formed normal to the new polarization direction. This was achieved through small changes in the scan length to ensure a perfect overlap between pulses in adjacent scan lines. For the remaining experiments, the polarization direction was chosen normal to the scanning direction so that LIPSS were parallel to the scanning direction. EDS and XRD analyses revealed no change in composition and crystallinity of the sample before and after the creation of LIPSS.

3.1 Effect of fluence

It was observed that below the fluence of 0.7 J/cm^2, no damage was visible on the surface of silicon. Above this fluence, LIPSS were formed and the structures were more prominent with deeper valleys as the fluence was further increased. In order to maximize the processing speed, the repetition rate was gradually increased from 10 to 640 kHz in steps. At each step, the power and the laser beam scan speed were increased to maintain the overlapping ratio and fluence required for the formation of LIPSS. It was observed that as long as the fluence was maintained, the scan speed had no impact on the structures formed. At 640 kHz, a scan speed of 4000 mm/s was used to create uniform LIPSS over an area of 4 cm by 4 cm.

SEM images revealed that the LIPSS had a period of 532 nm and a fill factor of 75 %. The depth of the channels was found to increase with increasing fluence. At 0.7 J/cm^2, ripples were faintly visible with minimal variation in height between crests and troughs. At 0.8 J/cm^2, highly uniform structures were obtained with no surface material removal. The periodic structures appeared to have flat top surface with filleted edges and deep narrow valleys. The depth of the valleys was determined through AFM imaging and found to range from 150 to 350 nm. Figure 3 shows SEM images of the highly periodic LIPSS created at a fluence of 0.8 J/cm^2. Figure 4 shows the progressive changes on the formed nanostructures with increasing laser

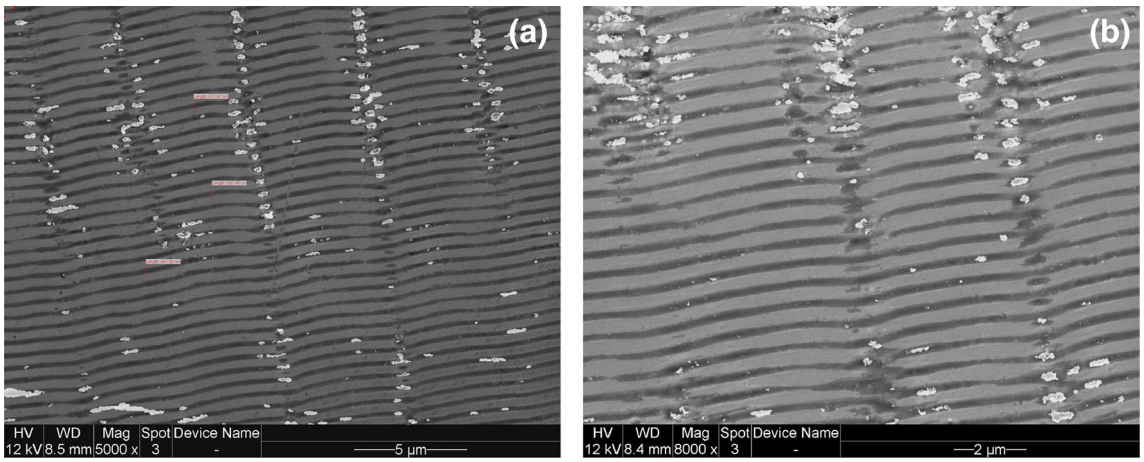

Fig. 3 SEM images of highly uniform LIPSS created at a fluence of 0.8 J/cm^2: **a** at ×5000 magnification, **b** at ×8000 magnification

fluence. At 1 J/cm^2, some material removal was observed and the deeper valleys were formed (Fig. 4b). The structures were still periodic, and the ripples were continuous with minor breakages. At 1.2 J/cm^2, the material removal caused breakage of the LIPSS and the structures were not continuous (Fig. 4d). The surface also appeared dull gray possibly due to mild oxidation on the surface and lower surface reflectance. The valleys however appeared deeper and smaller nanostructures were present on the surface. These nanostructures may have resulted from the sputtering of the parent silicon onto surrounding areas.

Visual observation of the textured silicon wafer revealed iridescence when viewed under a broadband light source as shown in Fig. 5. Different viewing angles measured from the horizontal resulted in different colors. This is attributed to structural coloration as a result of interference effects caused by the grating-like LIPSS. At 0°, the sample appeared gray as seen in Fig. 5a. As the angle was increased from 3.5° to 11.5° in steps of 2°, various colors were observed. This iridescent effect was seen only in structures created at fluence values between 0.7 and 1 J/cm^2. Above this fluence value, the surfaces began to appear dull and gray possibly due to increased light trapping.

3.2 Reflectance tests

Reflectance tests were conducted on the samples to study the effect of LIPSS on surface reflectance. Structures created at the same fluence value exhibited the same reflectance across the wavelength range of 200–1100 nm, irrespective of the scan speed and repetition rate used. Structures created with the same fluence appeared identical under the SEM and thus were expected to exhibit the same reflectance. Structures made with increasing fluence values exhibited a trend of decreasing average reflectance value. As the fluence was increased from 0.95 to 1.4 J/cm^2, the average reflectance over the wavelength range of 400–860 nm decreased from 25.79 to 19.84 %. As compared to the reflectance of bare silicon which was measured to be 35.93 % over the same wavelength range, a 44.8 % decrease in reflectance was achieved for the case of texturing at 1.4 J/cm^2. This drop is attributed to the increasing depth of channels and increasing irregularities on the surface.

At fluence values close to 0.8 J/cm^2, highly periodic and continuous LIPSS are formed with shallow valleys which are not very effective in trapping incident light. At higher fluence values up to 1 J/cm^2, the valley depth was found to increase and light was trapped more effectively. At a fluence of 1.1 J/cm^2, deep and continuous LIPSS were formed resulting in an average reflectance of 23.1 % corresponding to a 35.7 % decrease in average reflectance compared to bare silicon. At even higher fluence values up to 1.2 J/cm^2, deep valleys were created with irregularities due to material removal. This resulted in even lower reflectance values due to increased scattering of light below the surface of the material. Beyond this fluence value, the structures no longer appeared periodic. Deep craters and surface irregularities were formed which further enhanced scattering and light trapping below the surface, thus decreasing the average reflectance. Figure 6 shows the reflectance curves for structures created at different fluence values, across the wavelength range of 400–860 nm. A clear decreasing trend in reflectance is seen as the fluence is increased. Above this fluence, material removal causes severe damage to the surface.

The results indicate that random nanostructures are more effective in reducing surface reflection than periodic structures. As the fluence was increased and the structures transitioned from being highly periodic to random structures, there was a drop in average reflectance as well. This is in agreement with a study on disordered arrays of silicon

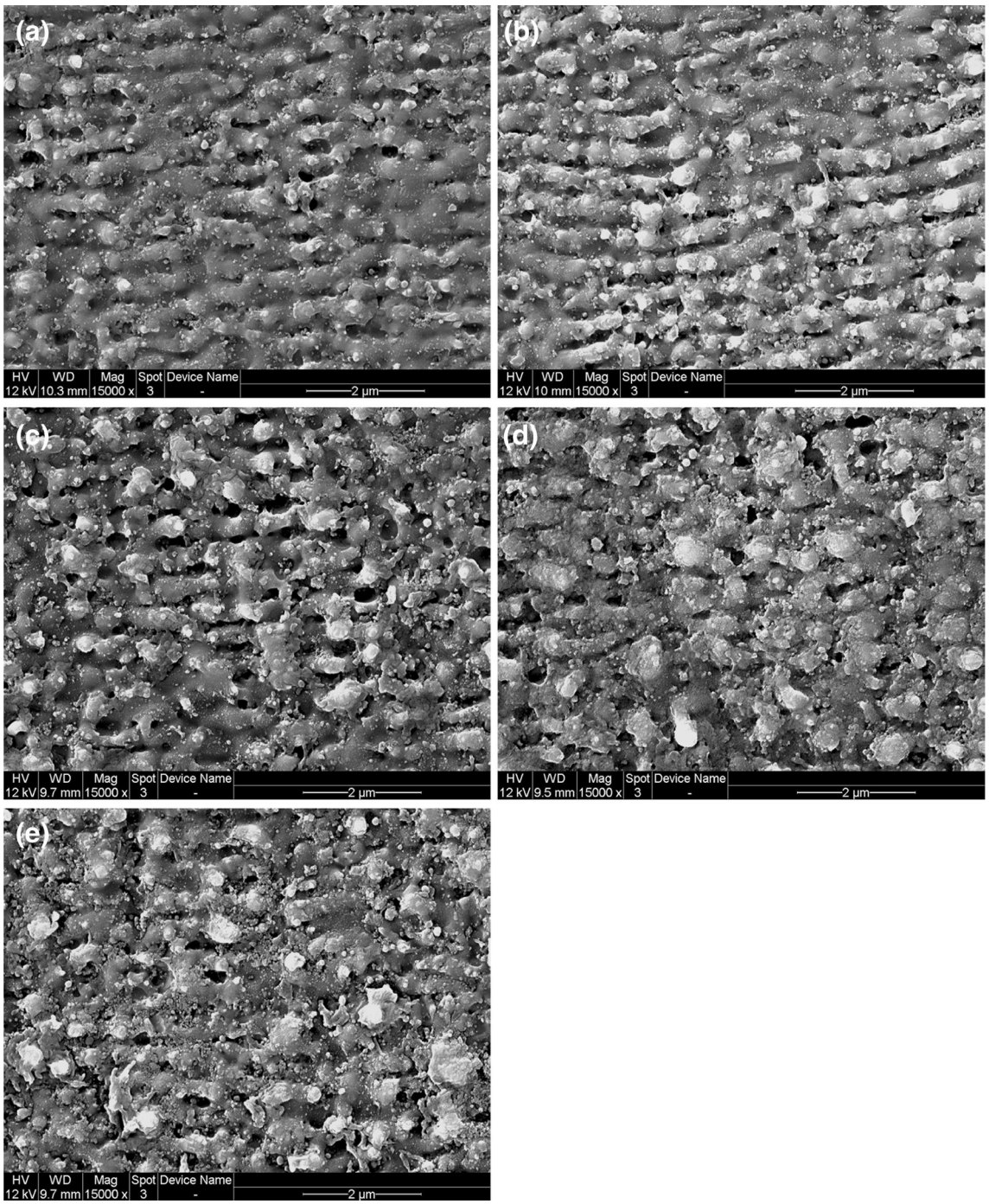

Fig. 4 SEM image of nanostructures created at a fluence of **a** 0.95 J/cm^2, **b** 1 J/cm^2, **c** 1.1 J/cm^2, **d** 1.2 J/cm^2, **e** 1.3 J/cm^2

nano-wires by Bao et al. [53], which also reported lower reflectance values with random surface structuring when compared with periodic uniform structures. To study the effects of a thin oxide layer on the textured surface, simulations were run and are discussed in Sect. 3.3 below. The results show that the effect of a thin oxide layer, if present, is negligible. Prior to reflectance testing, the samples were chemically cleaned in an ultrasonic bath. This ensures all organic impurities and surface particles which are loosely held are removed and do not influence the surface reflectance.

3.3 Simulation

In order to validate the experimental results and to study the predictability of the reflectance values of LIPSS,

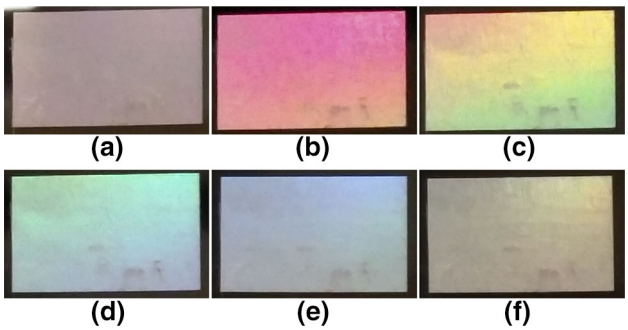

Fig. 5 Photographs showing iridescent effect of area covered with LIPSS when viewed at different angles to the horizontal: **a** 0°, **b** 3.5°, **c** 5.5°, **d** 7.5°, **e** 9.5°, **f** 11.5°

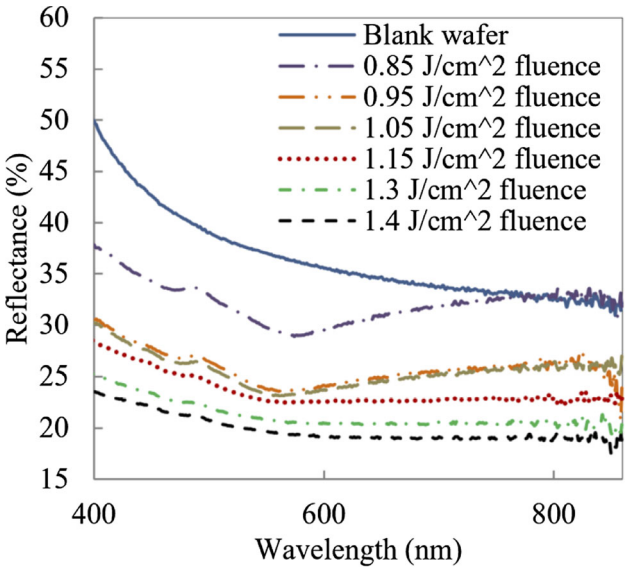

Fig. 6 Reflectance curves showing a decreasing trend in reflectance with increasing fluence values

computer simulations were conducted. In addition to this, simulations were conducted with different periodic geometries to study the effect of changing profiles on the reflectance. The commercial software Lumerical FDTD was used in this study. The software solves Maxwell's curl equations in non-magnetic materials. The governing equations are as follows:

$$\frac{\partial \vec{D}}{\partial t} = \nabla \times \vec{H}$$

$$\vec{D}(\omega) = \varepsilon_0 \varepsilon_r(\omega)\vec{E}(\omega)$$

$$\frac{\partial \vec{H}}{\partial t} = -\frac{1}{\mu_0}\nabla \times \vec{E}$$

where H, E and D are the magnetic, electric and displacement fields, respectively, while ε_r is the complex relative dielectric constant.

Simulations were performed to calculate the reflectance value over a unit cell of the structured silicon wafer. To validate the experimental results, the profile of the unit cell was modeled based on the AFM and SEM images of the structures formed in experiments. Since the structures were highly periodic, a single unit cell was sufficient to fully represent the surface structure. Also, a 2D simulation was sufficient to represent the structure as the grating cross section remained constant in the third dimension. The mesh size was set using the conformal mesh technology, which determines the required non-uniform mesh size to ensure convergence. A high-accuracy mesh setting was used, which provides a typical mesh size of 26–30 points per wavelength. The time step is automatically calculated from the simulation mesh size based on the Courant stability criterion. A periodic boundary condition was used along the x-axis (parallel to the silicon surface) to simulate a repetitive structure. For the y-axis, (normal to the surface) perfectly matched layer (PML) boundary condition was used to absorb unwanted reflections and prevent them from re-entering the simulation domain. A plane wave source was used to normally inject electromagnetic energy on the surface. The resultant reflectance spectrum was multiplied with the AM 1.5G solar spectrum to simulate sunlight incident on the surface. Comparative studies between experiments and simulations were done for the periodic structures formed at a fluence value of 0.85 J/cm^2. The fill factor, defined as the percentage of the grating period consisting of silicon, was measured to be 75 %, and the depth was 350 nm. The top surfaces of the ripples appeared flat, and the edges were rounded.

A good match between experimental and simulated values of reflectance was obtained as can be seen from Fig. 7a. LIPSS formed using the 1064 nm wavelength laser were also subjected to reflectance testing using the spectrophotometer. These results were also compared with FDTD simulations. The fill factor was measured to be 75 %, and the depth of valleys was measured to be 350 nm. Once again a good agreement between experimental and simulated results can be seen in Fig. 7b.

Simulations were conducted to study the effect on reflectance due to an oxide layer on surface structures. It was found that the effects were negligible for oxide layers smaller than 10 nm as seen in Fig. 8 which shows the case of 532 nm period simple grating with a valley depth of 300 nm. An oxide layer, if at all, present is not likely to affect the average reflectance since it is expected to be very thin for such small exposure times to high temperatures.

Different grating profiles were compared through simulations to study their effects on reflectance. Four profiles were compared, namely a simple grating having a rectangular profile, grating with a rounded top, grating with an elliptical profile and a grating with a flat top having curved

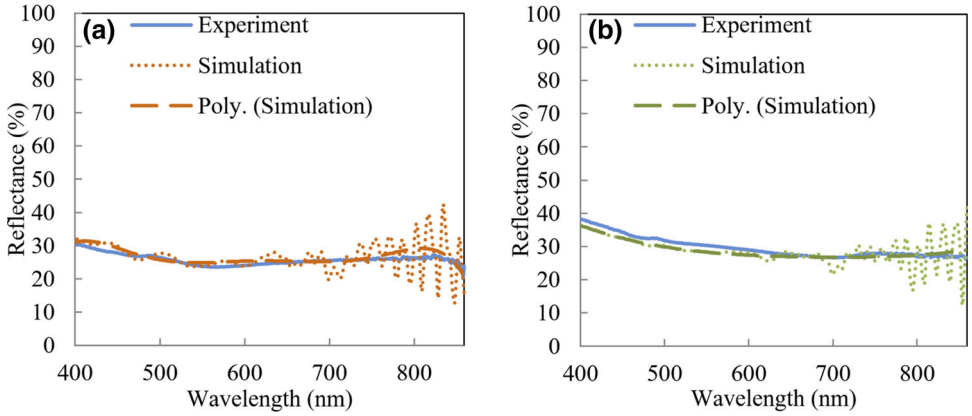

Fig. 7 Comparison between experimental and simulated reflectance curves for LIPSS having a period of **a** 532 nm, **b** 1064 nm

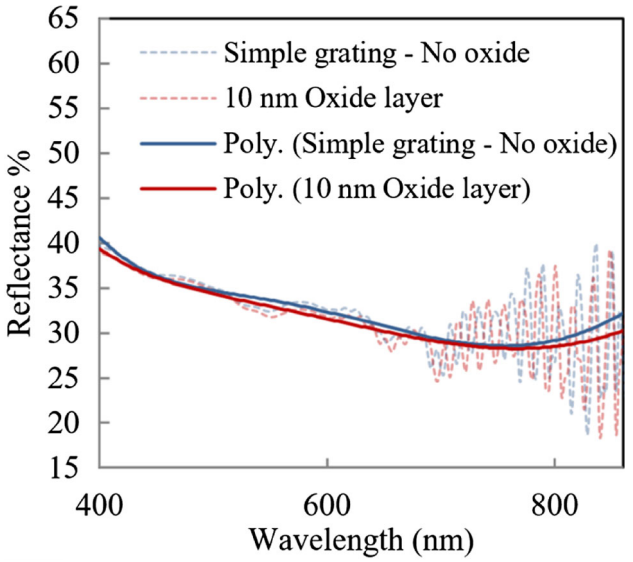

Fig. 8 Reflectance curves for simple grating structures with and without an oxide layer

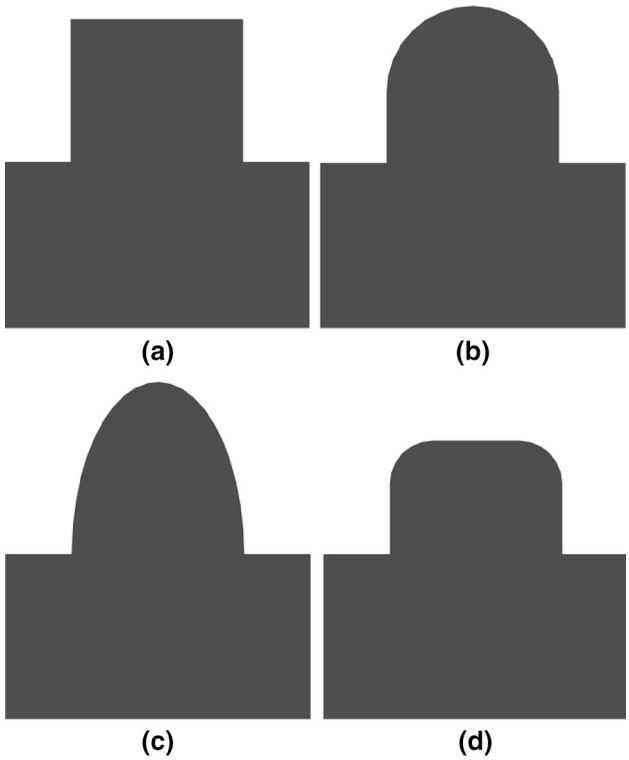

Fig. 9 Profiles used in reflectance simulation: **a** simple grating, **b** rounded top, **c** elliptical profile and **d** flat top with curved edges

edges. These profiles were chosen as they were most similar to the experimental LIPSS obtained. Figure 9 shows the cross-sectional view of the different profiles modeled. Although the profiles appear similar, their effect on reflectance varies significantly. The different profiles chosen were each simulated for multiple valley depths (varied from 200 to 400 nm in 50 nm intervals) and fill factors (varied from 55 to 75 % in 5 % intervals), and the results were analyzed. The elliptical profile resulted in the lowest average reflectance among the chosen profiles for all valley depths greater than 250 nm and all fill factors. The gratings with flat tops having curved edges resulted in the highest average reflectance values. The cases of simple grating and round top gratings were intermediate to the previous two cases and were dependent on the valley depth. For small valley depths of 200–250 nm, simple gratings provided lower average reflectance values while at higher valley depths of 300–400 nm, gratings with round top resulted in lower average reflectance. This can be seen in Fig. 10a for the case of 65 % fill factor.

Simulations were also performed to study the effect of fill factor on the reflectance. The fill factor was varied from 50 to 80 % in steps, by increasing the profile width while keeping the period and the depth of structures constant. This range was chosen as experimental data of LIPSS fill factors ranged between 60 and 75 %. It was found that a fill factor of 50 % was the most effective in suppressing surface reflectance. For fill factors higher than 50 %, it was found that as the fill factor was increased, the average reflectance also increased as shown in Fig. 10b. Figure 10b

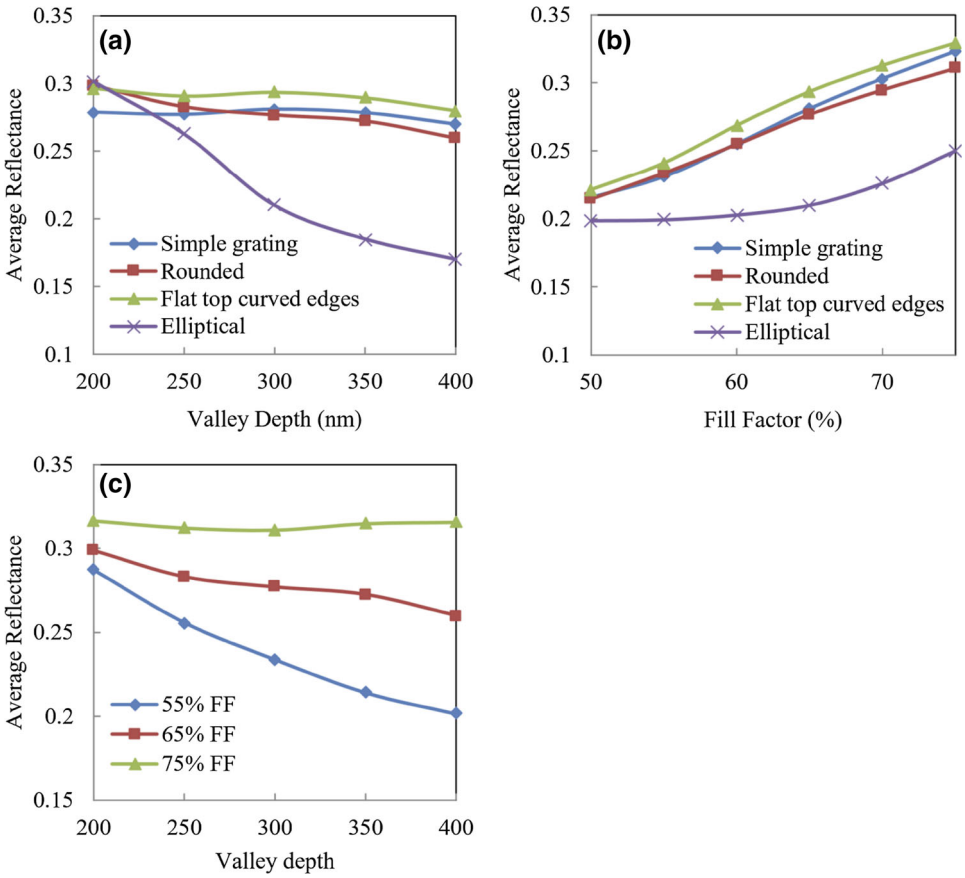

Fig. 10 **a** Average reflectance versus valley depth for different profiles for the case of 65 % fill factor, **b** average reflectance versus fill factor for different profiles for the case of 300 nm valley depth, **c** sensitivity of average reflectance value to changes in valley depth for different fill factors

shows the case of a constant valley depth of 300 nm. For all profile types, there is an increase in average reflectance with higher fill factors.

The effect of changing the valley depth was also studied through simulations. The depth of the LIPSS valleys was varied from 200 to 400 nm in steps. This range was chosen as experimental data of LIPSS valley depths ranged between these values. It was found that the fill factor influenced the effect of changes in valley depth on the reflectance. At lower fill factors of 50–60 %, deeper valleys resulted in lower reflectance values. This is explained by the fact that deeper valleys cause increased scattering and trap light more effectively. At slightly higher fill factors of 60–70 %, a similar trend of decreasing average reflectance values with increasing valley depths was observed. However, it was observed that the average reflectance was less sensitive to changes in valley depth. At even higher fill factors ranging from 70 to 80 %, the reflectance remained almost constant as the valley depth was increased from 200 to 400 nm. In some cases, even a small increase in average reflectance of up to 1 % was observed over the wavelength range of 400–1100 nm. This is attributed to the fact that at high fill factors, the incoming light radiation is incident onto a larger front surface area as compared to the case of a lower fill factor. This would cause an increase in the surface reflectance. The sensitivity of average reflectance to increasing valley depth reduced as the fill factor increased as can be seen in Fig. 10c. Figure 10c represents the case of structures with a rounded top, and the same trend was observed for all the different profiles simulated.

4 Conclusion

By utilizing the light trapping properties of periodic grating structures, silicon wafers with average reflectance values of 23.1 % were fabricated by texturing the surface with a picosecond laser. These structures were created at high laser scanning speeds of 4000 mm/s and low pulse overlapping ratios of 60 %. This method provides an inexpensive and rapid process to create low-reflectance silicon wafers which can be used in photovoltaic applications. A decreasing trend in average reflectance was observed when the LIPSS were created with increasing fluence values up to 1.4 J/cm^2. Beyond this value, material ablation was observed. The experimentally achieved reflectance values for highly periodic LIPSS have been validated through FDTD simulations that displayed a high degree of predictability. Various periodic geometries were simulated to

study their impact on surface reflectance. Elliptical profiles resulted in the lowest average reflectance among the profiles simulated. The effects of changing valley depth and fill factor in each of these structures were also studied, showing that higher fill factors resulted in higher average reflectance values. A steady drop in sensitivity of average reflectance to change in valley depth is reported as the fill factor is increased above 50 %.

Acknowledgments The authors wish to gratefully acknowledge the financial support provided for this study by the National Science Foundation (Grant Nos. CMMI-1030786 and CMMI-1300930).

References

1. M.A. Green, K. Emery, Y. Hishikawa, W. Warta, E.D. Dunlop, Solar cell efficiency tables (Version 45). Prog. Photovolt. Res. Appl. **23**, 1–9 (2015)
2. J.I. Gittleman, E.K. Sichel, H.W. Lehmann, R. Widmer, Textured silicon: a selective absorber for solar thermal conversion. Appl. Phys. Lett. **35**, 742 (1979). doi:10.1063/1.90953
3. A.W. Smith, A. Rohatgi, A new texturing geometry for producing high efficiency solar cells with no antireflection coatings. Sol. Energy Mater. Sol. Cells **29**, 51–65 (1993)
4. S. Winderbaum, O. Reinhold, F. Yun, Reactive ion etching (RIE) as a method for texturing polycrystalline silicon solar cells. Sol. Energy Mater. Sol. Cells **46**, 239–248 (1997)
5. D.H. Macdonald, A. Cuevas, M.J. Kerr, C. Samundsett, D. Ruby, S. Winderbaum, A. Leo, Texturing industrial multicrystalline silicon solar cells. Sol. Energy **76**, 277–283 (2004)
6. L. Hu, G. Chen, Analysis of optical absorption in silicon nanowire arrays for photovoltaic applications. Nano Lett. **7**(11), 3249–3252 (2007). doi:10.1021/nl071018b
7. C.H. Sun, P. Jiang, B. Jiang, Broadband moth-eye antireflection coatings on silicon. Appl. Phys. Lett. **92**, 061112 (2008). doi:10.1063/1.2870080
8. A. Mavrokefalos, S.E. Han, S. Yerci, M.S. Branham, G. Chen, Efficient light trapping in inverted nanopyramid thin crystalline silicon membranes for solar cell applications. Nano Lett. **12**, 2792–2796 (2012). doi:10.1021/nl2045777
9. K.X. Wang, Z. Yu, V. Liu, Y. Cui, S. Fan, Absorption enhancement in ultrathin crystalline silicon solar cells with antireflection and light-trapping nanocone gratings. Nano Lett. **12**, 1616–1619 (2012). doi:10.1021/nl204550q
10. J. Zhu, C.M. Hsu, Z. Yu, S. Fan, Y. Cui, Nanodome solar cells with efficient light management and self-cleaning. Nano Lett. **10**, 1979–1984 (2010). doi:10.1021/nl9034237
11. R.C. Enger, S.K. Case, Optical elements with ultrahigh spatial-frequency surface corrugations. Appl. Opt. **22**(20), 15 (1983)
12. T.K. Gaylord, W.E. Baird, M.G. Moharam, Zero-reflectivity high spatial-frequency rectangular-groove dielectric surface-relief gratings. Appl. Opt. **25**(24), 15 (1986)
13. Y. Ono, Y. Kimura, Y. Ohta, N. Nishida, Antireflection effect in ultrahigh spatial-frequency holographic relief gratings. Appl. Opt. **26**(6), 15 (1987)
14. T.K. Gaylord, E.N. Glytsis, M.G. Moharam, Zero-reflectivity homogeneous layers and high spatial frequency surface-relief gratings on lossy materials. Appl. Opt. **26**(15), 1 (1987)
15. D.H. Raguin, G.M. Morris, Analysis of antireflection-structured surfaces with continuous one-dimensional surface profiles. Appl Opt (1993). doi:10.1364/AO.32.002582
16. S. Chattopadhyay, Y.F. Huang, Y.J. Jen, A. Ganguly, K.H. Chen, L.C. Chen, Anti-reflecting and photonic nanostructures. Mater. Sci. Eng. R Rep. **69**, 1–35 (2010)
17. Y. Kanamori, M. Sasaki, K. Hane, Broadband antireflection gratings fabricated upon silicon substrates. Opt. Lett. **24**(20), 1422–1424 (1999)
18. C. David, P. Haberling, M. Schnieper, J. Sochtig, C. Zschokke, Nano-structured anti-reflective surfaces replicated by hot embossing. Microelectron. Eng. **61–62**, 435–440 (2002)
19. Y. Kanamori, E. Roy, Y. Chen, Antireflection sub-wavelength gratings fabricated by spin-coating replication. Microelectron. Eng. **78–79**, 287–293 (2005)
20. M. Birnbaum, Semiconductor surface damage produced by ruby lasers. J. Appl. Phys. **36**, 3688 (1965). doi:10.1063/1.1703071
21. J.F. Young, J.S. Preston, H.M. van Driel, J.E. Sipe, Laser-induced periodic surface structure. II. Experiments on Ge, Si, Al, and brass. Phys. Rev. B **27**, 1155 (1983)
22. W.J. Wang, Y.F. Lu, C.W. An, M.H. Hong, T.C. Chong, Controllable periodic structures on silicon wafer by CO_2 laser irradiation. Appl. Surf. Sci. **186**(1–4), 594–598 (2002)
23. E.M. Hsu, T.H.R. Crawford, H.F. Tiedje, H.K. Haugen, Periodic surface structures on gallium phosphide after irradiation with 150 fs–7 ns laser pulses at 800 nm. Appl. Phys. Lett. **91**, 111102 (2007). doi:10.1063/1.2779914
24. N.R. Isenor, CO_2 laser-produced ripple patterns on Ni_xP_{1-x} surfaces. Appl. Phys. Lett. **31**, 148 (1977). doi:10.1063/1.89633
25. S.E. Clark, D.C. Emmony, Ultraviolet-laser-induced periodic surface structures. Phys. Rev. B **40**(4), 1 (1989)
26. A.V. Demchuk, V.A. Labunov, Surface morphology and structure modification of silicon layers induced by nanosecond laser radiation. Appl. Surf. Sci. **86**, 353–358 (1995)
27. P.M. Fauchet, A.E. Siegman, Surface ripples on silicon and gallium arsenide under picosecond laser illumination. Appl. Phys. Lett. **40**, 824 (1982). doi:10.1063/1.93274
28. X. Zhu, H. Zhu, D. Liu, Y. Huang, X. Wang, H. Yu, S. Wang, X. Lin, P. Han, Picosecond laser microstructuring for black silicon solar cells. Adv. Mater. Res. **418–420**, 217–221 (2012)
29. A.M. Ozkan, A.P. Malshe, T.A. Railkar, W.D. Brown, Femtosecond laser-induced periodic structure writing on diamond crystals and microclusters. Appl. Phys. Lett. **75**(23), 6 (1999)
30. B. Tan, K. Venkatakrishnan, A femtosecond laser-induced periodical surface structure on crystalline silicon. J. Micromech. Microeng. **16**, 1080–1085 (2006)
31. E.L. Gurevich, Self-organized nanopatterns in thin layers of superheated liquid metals. Phys. Rev. E **83**, 031604 (2011). doi:10.1103/PhysRevE.83.031604
32. A.Y. Vorobyev, C. Guo, Femtosecond laser nanostructuring of metals. Opt. Express **14**(6), 2164 (2006)
33. M. Henyk, N. Vogel, D. Wolfframm, A. Tempel, J. Reif, Femtosecond laser ablation from dielectric materials: Comparison to arc discharge erosion. Appl. Phys. A **69**(Suppl.), S355–S358 (1999)
34. F. Costache, M. Henyk, J. Reif, Modification of dielectric surfaces with ultra-short laser pulses. Appl. Surf. Sci. **186**(1–4), 352–357 (2002)
35. Y. Li, V.A. Stoica, L. Endicott, G. Wang, H. Sun et al., Femtosecond laser-induced nanostructure formation in Sb_2Te_3. Appl. Phys. Lett. **99**, 121903 (2011). doi:10.1063/1.3634014
36. C. Daniel, J. Drummond, R.A. Giordano, Improving flexural strength of dental restorative ceramics using laser interference direct structuring. J. Am. Ceram. Soc. **91**(10), 3455–3457 (2008)
37. Y. Xing, J. Deng, Y. Lian, X. Feng, Femtosecond pulsed laser nanotexturing of Al_2O_3/TiC ceramic. Laser Phys. **23**, 066002 (2013). doi:10.1088/1054-660X/23/6/066002

38. E. Rebollar, S. Pérez, J.J. Hernández, I. Martín-Fabiani, D.R. Rueda, T.A. Ezquerra, M. Castillejo, Ultraviolet and infrared femtosecond laser induced periodic surface structures on thin polymer films. Appl. Phys. Lett. **100**, 041106 (2012). doi:10.1063/1.3679103
39. E. Rebollar, S. Pérez, J.J. Hernández, I. Martín-Fabiani, D.R. Rueda, T.A. Ezquerra, M. Castillejo, Assessment and formation mechanism of laser-induced periodic surface structures on polymer spin-coated films in real and reciprocal space. Langmuir **27**(9), 5596–5606 (2011). doi:10.1021/la200451c
40. J. Bonse, H. Sturm, D. Schmidt, W. Kautek, Chemical, morphological and accumulation phenomena in ultrashort-pulse laser ablation of TiN in air. Appl. Phys. A **71**, 657–665 (2000). doi:10.1007/s003390000585
41. A. Borowiec, H.K. Haugen, Subwavelength ripple formation on the surfaces of compound semiconductors irradiated with femtosecond laser pulses. Appl. Phys. Lett. **82**(25), 23 (2003)
42. F. Costache, S. Kouteva-Arguirova, J. Reif, Sub–damage–threshold femtosecond laser ablation from crystalline Si: surface nanostructures and phase transformation. Appl. Phys. A **79**, 1429–1432 (2004). doi:10.1007/s00339-004-2803-y
43. J. Bonse, M. Munz, H. Sturm, Structure formation on the surface of indium phosphide irradiated by femtosecond laser pulses. J. Appl. Phys. **97**, 013538 (2005). doi:10.1063/1.1827919
44. T. Tomita, Y. Fukumori, K. Kinoshita, S. Matsuo, S. Hashimoto, Observation of laser-induced surface waves on flat silicon surface. Appl. Phys. Lett. **92**, 013104 (2008). doi:10.1063/1.2828983
45. Y. Han, S. Qu, Uniform self-organized grating fabricated by single femtosecond laser on dense flint (ZF6) glass. Appl. Phys. A **98**, 167–170 (2010). doi:10.1007/s00339-009-5443-4
46. X. Jia, T.Q. Jia, Y. Zhang, P.X. Xiong, D.H. Feng, Z.R. Sun, J.R. Qiu, Z.Z. Xu, Periodic nanoripples in the surface and subsurface layers in ZnO irradiated by femtosecond laser pulses. Opt. Lett. **35**(8), 1248–1250 (2010)
47. E.M. Hsu, T.H.R. Crawford, C. Maunders, G.A. Botton, H.K. Haugen, Cross-sectional study of periodic surface structures on gallium phosphide induced by ultrashort laser pulse irradiation. Appl. Phys. Lett. **92**, 221112 (2008). doi:10.1063/1.2936865
48. Y. Shimotsuma, P.G. Kazansky, J. Qiu, K. Hirao, Self-organized nanogratings in glass irradiated by ultrashort light pulses. Phys. Rev. Lett. **91**(24), 12 (2003). doi:10.1103/PhysRevLett.91.247405
49. J. Reif, F. Costache, M. Henyk, S.V. Pandelov, Ripples revisited: non-classical morphology at the bottom of femtosecond laser ablation craters in transparent dielectrics. Appl. Surf. Sci. **197–198**(30), 891–895 (2002). doi:10.1016/S0169-4332(02)00450-6
50. J.E. Sipe, J.F. Young, J.S. Preston, H.M. van Driel, Laser-induced periodic surface structure. I. Theory. Phys. Rev. **27**(2), 1141–1154 (1983)
51. J.W. Yao, C.Y. Zhang, H.Y. Liu, Q.F. Dai, L.J. Wu, S. Lan, A.V. Gopal, V.A. Trofimov, T.M. Lysak, High spatial frequency periodic structures induced on metal surface by femtosecond laser pulses. Opt. Express **20**(2), 905–911 (2012). doi:10.1364/OE.20.000905
52. A.Y. Vorobyev, C. Guo, Antireflection effect of femtosecond laser-induced periodic surface structures on silicon. Opt. Express **19**(S5), A1036 (2011)
53. H. Bao, X. Ruan, Optical absorption enhancement in disordered vertical silicon nanowire arrays for photovoltaic applications. Opt. Lett. **35**(20), 3378–3380 (2010)